



**HAL**  
open science

## Mid-infrared observations of O-type stars: spectral morphology

Wagner L. F. Marcolino, Jean-Claude Bouret, Thierry Lanz, Donovan S. Maia, Marc Audard

► **To cite this version:**

Wagner L. F. Marcolino, Jean-Claude Bouret, Thierry Lanz, Donovan S. Maia, Marc Audard. Mid-infrared observations of O-type stars: spectral morphology. *Monthly Notices of the Royal Astronomical Society*, 2017, 470 (3), pp.2710 - 2722. 10.1093/mnras/stx1191 . hal-01784502

**HAL Id: hal-01784502**

**<https://hal.science/hal-01784502>**

Submitted on 10 May 2018

**HAL** is a multi-disciplinary open access archive for the deposit and dissemination of scientific research documents, whether they are published or not. The documents may come from teaching and research institutions in France or abroad, or from public or private research centers.

L'archive ouverte pluridisciplinaire **HAL**, est destinée au dépôt et à la diffusion de documents scientifiques de niveau recherche, publiés ou non, émanant des établissements d'enseignement et de recherche français ou étrangers, des laboratoires publics ou privés.

# Mid-infrared observations of O-type stars: spectral morphology <sup>\*</sup>

W. L. F. Marcolino<sup>1†</sup>, J.-C. Bouret<sup>2</sup>, T. Lanz<sup>3</sup>, D. S. Maia<sup>1</sup>, and M. Audard<sup>4</sup>

<sup>1</sup>Universidade Federal do Rio de Janeiro, Observatório do Valongo, Ladeira Pedro Antônio, 43, Rio de Janeiro, Brasil

<sup>2</sup>Aix Marseille Univ, CNRS, LAM, Laboratoire d'Astrophysique de Marseille, Marseille, France

<sup>3</sup>Observatoire de la Côte d'Azur, Nice, France

<sup>4</sup>Department of Astronomy, University of Geneva, ch. d'Ecogia 16, CH-1290 Versoix, Switzerland

Last updated 2017 April; in original form 2017 March

## ABSTRACT

We present mid-infrared observations for a sample of 16 O-type stars. The data were acquired with the NASA *Spitzer Space Telescope*, using the IRS instrument at moderate resolution ( $R \sim 600$ ), covering the range  $\sim 10 - 37 \mu\text{m}$ . Our sample includes early, mid and late O supergiants and dwarfs. We explore for the first time their mid-IR spectral morphology in a quantitative way. We use NLTE expanding atmosphere models to help with line identifications, analyze profile contributions and line-formation regions. The O supergiants present a rich emission line spectra. The most intense features are from hydrogen -  $6\alpha$ ,  $7\alpha$ , and  $8\alpha$  - which have non-negligible contributions of He I or He II lines, depending on the spectral type. The spectrum of early O supergiants is a composite of H I and He II lines, He I lines being absent. On the other hand, late O supergiants present features composed mainly by H I and He I lines. All emission lines are formed throughout the stellar wind. We found that O dwarfs exhibit a featureless mid-IR spectrum. Two stars of our sample exhibit very similar mid-IR features, despite having a very different optical spectral classification. The analysis of O-type stars based on mid-IR spectra alone to infer spectral classes or to estimate physical parameters may thus be prone to substantial errors. Our results may therefore inform spectroscopic observations of massive stars located in heavily obscured regions and help establish an initial framework for observations of massive stars using the Mid-Infrared Instrument on the *James Webb Space Telescope*.

**Key words:** massive stars – O stars – mid-infrared spectroscopy – stellar winds – atmosphere models

## 1 INTRODUCTION

Massive O stars have been extensively studied in the last decades through the comparison of synthetic spectra with high-resolution spectroscopic data. Most of such investigations found in the literature focus on ground-based optical observations, and some also include satellite ultraviolet (UV) observations. Depending on the luminosity class, both the photosphere and wind of an O star can be detected in the optical (e.g., in early supergiants). However, the major energy output from massive stars is in the UV region, where most stellar wind diagnostics can be found.

After the first rocket experiments (Morton 1967) and

with the early satellite missions in the UV (e.g., *Copernicus*, *IUE*), a variety of P-Cygni line profiles of different ions was revealed for the first time (e.g., N v  $\lambda\lambda 1239, 1243$ , O v  $\lambda 1371$ , Si iv  $\lambda\lambda 1394, 1403$ , C iv  $\lambda\lambda 1548, 1551$ , He II  $\lambda 1640$ , and N iv  $\lambda 1718$ ). It was soon discovered that the UV morphological properties of the O-type stars is strongly correlated to their optical spectral classifications (Walborn & Panek 1984). Since then, these lines were continuously used to infer the mass-loss rates and terminal wind velocities of O stars of various spectral types (Howarth & Prinja 1989). In addition, detailed analyses of UV data revealed several new physical informations (e.g., NACs, superionization, clumping; Prinja & Howarth 1986; Bouret et al. 2005) and provided ways to check parameters inferred from optical analyses (e.g., effective temperatures; Crowther et al. 2002).

Compared to the UV and optical studies, there are relatively few high-resolution observations of O stars at longer wavelengths. In the infrared (IR), the energetic output of O-

<sup>\*</sup> Based on observations with the NASA *Spitzer Space Telescope*, which is operated by the Jet Propulsion Laboratory (JPL), California Institute of Technology (Caltech), under a contract with National Aeronautics and Space Administration (NASA).

† Contact e-mail: wagner@astro.ufrj.br

**Table 1.** Log of the *Spitzer Space Telescope* mid-IR observations. Exposure times include target plus sky background subtraction.

Star	Spectral type	Total exposure time (s)		Obs. Date	Note
		IRS/SH	IRS/LH		
HD 66811	O4If+	38	50	2007-10-19 2007-10-23	$\zeta$ Puppis
HD 190429A	O4If+	218	1935	2004-06-26	
HD 188001	O7.5Iaf	244	1935	2006-11-14 2007-06-13	9 Sge
HD 207198	O8.5II	126	967	2006-10-18	
HD 30614	O9.5Iab	63	117	2006-10-18 2007-10-03	$\alpha$ Cam
HD 188209	O9.5Iab	244	1935	2006-10-18	
HD 209975	O9.5Ib	126	488	2006-09-15	19 Cep
HD 195592	O9.7Ia	126	244	2006-10-18 2006-11-13	
HD 46223	O4V((f))	488	3869	2007-04-27	
HD 46150	O5V((f))	488	2902	2007-04-27	
HD 199579	O6V((f))	244	967	2007-06-18	
HD 206267	O6.5V((f))	244	488	2006-10-18	
HD 47839	O7V((f))	488	4837	2007-04-27 2007-05-02	15 Mon
HD 209481	O9V	488	3869	2006-10-18	LZ Cep
HD 214680	O9V	488	4837	2007-08-03 2007-09-02	10 Lac
HD 38666	O9.5V	488	3869	2007-10-06	$\mu$ Col

type stars is considerably weaker than in the optical and UV regions. Moreover, depending on the IR band, several observational difficulties appear (e.g., telluric contamination, sky and thermal emission). Nonetheless, near and mid-IR data present obvious advantages in some specific contexts. For example, at various Galactic locations, the visual extinction is very large, reaching  $A_V \sim 20 - 30$  (e.g., obscured H II regions; Galactic center), and the analysis and interpretation of J, H and K band spectra remains the best opportunity. In this context, [Lenorzer et al. \(2004\)](#) were able to show that the He I-II line ratios in the near-IR correlate well with the line ratios in the optical spectrum that are used for spectral classification (see also [Hanson et al. 1996](#)). Soon after, [Repolust et al. \(2005\)](#) demonstrated for a sample of OB stars that photospheric and wind parameters derived from the near-IR alone matched well the ones derived from the optical (within error bars). That is, *a priori* one can obtain accurate physical parameters of OB stars which are not accessible at visual or UV wavelengths because of high extinction.

However, we should note that a direct spectral classification or derivation of physical parameters based only on the infrared is not problem-free. For instance, [Conti et al. \(1995\)](#) found two Of stars with K band spectra typical of Wolf-Rayet stars (WN type), despite having normal optical and UV characteristics found in the Of class. By analyzing evolved massive stars, [Morris et al. \(1996\)](#) reported a similar problem, where objects from a certain group -WNL, Of, Of/WN, Be, B[e] or LBV - can be classified as a member of another class if one relies uniquely on the  $2\mu\text{m}$  spectra. An analogous issue is pointed out again in the present paper.

Combined with other spectral regions, long wavelength data can provide valuable additional constraints on important physical parameters. In the near-IR for example, the Br $\alpha$  line emerged as an important mass-loss rate diagnostic

in O stars ([Lenorzer et al. 2004](#); [Najarro et al. 2011](#)). The IR and radio region have also long been known to provide mass-loss values through continuum flux excesses ([Wright & Barlow 1975](#)). However, given the very low fluxes, radio band studies are usually restricted to the brightest objects. More recently, radio plus IR and optical data were used by [Puls et al. \(2006\)](#) to evidence strong constraints on the radial stratification of wind clumping in O stars (density inhomogeneities). Such multi-wavelength investigations are crucial to address the stellar and wind properties of massive stars. Uncertainties on stellar parameters can be reduced and model limitations might become clear by using as many line and continuum diagnostics as possible.

In this work, we present mid-IR observations of O stars and discuss their spectral morphology for the first time. The data were acquired with the IRS instrument on-board the NASA *Spitzer Space Telescope*. Our sample consists of 16 stars, comprising late, mid and early dwarfs and supergiants. We describe their mid-IR spectral morphology with the aid of NLTE stellar atmosphere models and complementary ultraviolet and optical data. We present line identifications, equivalent width measurements, profile formation regions and ion contributions. There are clear differences among the spectral types. O dwarfs present featureless atmospheric spectra. In supergiants, the mid-IR lines - essentially from hydrogen and helium - increase considerably in strength from late to early supergiants. Interestingly, two stars of our sample present very similar mid-IR spectra, despite having different optical spectra (spectral types). In Sect. 2, we start by presenting our sample along with the observational details. In Sect. 3, we show the observed spectra and discuss the mid-IR spectral morphology in detail. Our main conclusions are summarized in Sect. 4.

## 2 OBSERVATIONS

We used the IRS instrument onboard the NASA *Spitzer Space Telescope* to obtain mid-infrared high-resolution spectra for a sample of 16 O stars (PI T. Lanz, program 30030). The Short-High (SH) and Long-High (LH) modules were used (Houck et al. 2004). Both are cross-dispersed echelle spectrographs which provide a wavelength coverage of  $\sim 9.9 - 19.6\mu\text{m}$  and  $\sim 18.7 - 37.2\mu\text{m}$ , respectively. The detectors are  $128 \times 128$  pixel Si:As blocked impurity band arrays, with 2.3 arcsec per pixel (SH) and 4.5 arcsec per pixel (LH). The exposure times were estimated to aim for signal-to-noise ratios of about 150 and 50 with the SH and LH modules, respectively. The data reduction was performed from the processed pipeline data, using post-BCD tools and the SPICE package (Teplitz & Brinkworth 2011). The final spectra were obtained by co-adding the different sub-exposures (2 to 4 individual exposures for SH and LH, respectively) and by merging the different orders with an IDL routine. They were all normalized by polynomial fits to the continua, each specified by a careful selection of points in continuum windows. Our sample consists of 8 dwarfs and 8 supergiants, comprising late, mid and early types. The stars and corresponding spectral classes (Sota et al. 2014) are presented in Table 1. Total exposure times for each module are indicated, including time used for sky background subtraction. For HD 190429A, we did not repeat observations in the SH range and made use of previous IRS calibration observations, namely, from *AOR10021376*.

In order to achieve our goals, we also use high-resolution ultraviolet and optical observations to further analyze the mid-infrared region quantitatively by means of sophisticated atmosphere models (see Section 3). In the optical, we used public and own data from the FEROS (R  $\sim 48000$ ), NARVAL (Telescope Bernard-Lyot; R  $\sim 65000$ ), ESPADONS (CFHT; R  $\sim 68000$ ), and ELODIE (OHP; R  $\sim 42000$ ) spectrographs. In the ultraviolet, we focused on SWP spectra from the *International Ultraviolet Explorer* satellite.

## 3 MID-IR SPECTRAL MORPHOLOGY

Previous mid-IR spectra of O-type stars were shown by Ardila et al. (2010) in their *Spitzer Atlas of Stellar Spectra* (SASS). The atlas contains a total of 159 objects of several spectroscopic types, out of which 12 objects are O-type stars. It is most complete at spectral types later than the G type, for luminosity classes V (dwarfs) and III (giants). The O stars are not analyzed in detail, neither qualitatively nor quantitatively. Ardila et al. (2010) only emphasized that the spectra contain emission lines that are typical of wind or circumstellar material. The resolving power of the SASS observations is  $\sim 60 - 130$ , with the low-resolution mode of the IRS, that is a factor of about 5 to 10 lower than the resolution of the spectra shown here. Previous observations with other space observatories (e.g., *ISO*, *IRAS*) are also of lower resolution, focusing mainly in spectral types and objects other than O stars (see e.g., the compilation by Hodge et al. 2004).

In order to provide a robust morphological analysis of the spectra, we relied on stellar atmosphere models computed with the code CMFGEN (Hillier & Miller 1998). We

provide line identifications, equivalent width measurements ( $W_\lambda$ ), compute individual ion contributions and line formation regions to fully characterize the mid-IR spectrum of O stars for the first time. We refer the reader to Bouret et al. (2012) for a detail description of the code and a canonical approach for a thorough analysis of massive stars. For several stars, we did not start the quantitative analysis from scratch. Initial models were taken from previous investigations by our group (Martins et al. 2015a; Martins et al. 2015b; Bouret et al. 2012). For completeness, we present the photospheric and wind parameters of the final models in Table A1.

A detailed discussion about the models, their sensitivity to the parameters and the potential of mid-IR spectra to constrain the physical properties, especially useful in the context of the arrival of JWST, will be presented in a forthcoming paper. Here, we focus on the mid-IR morphology. We present and discuss the spectra of our sample below, starting with the O supergiant stars.

### 3.1 O supergiants

The spectra of the O supergiants of our sample are displayed in Figs. 1 and 2. For clarity, they were normalized and offset by a constant. We cut data beyond  $\sim 31 \mu\text{m}$ , due to very poor signal-to-noise ratio.

The observed spectra are characterized by a wealth of emission lines. The identification of these features was made more reliable thanks to the synthetic spectra computed with CMFGEN, which agree well for the whole sample with observations throughout the entire spectral range. We stress that this is truly remarkable since the parameters of the models were constrained from the analysis of the optical and UV spectra. Although models are not the focus of the present paper, we illustrate this excellent agreement in Fig. A1 using the O4If+ star  $\zeta$  Puppis as an example. The high fidelity of the synthetic spectra, over such a broad wavelength range, is a major achievement of stellar atmosphere modeling<sup>1</sup>.

The most intense spectral lines in the mid-IR spectrum of the O-type supergiants correspond to wavelengths of the H I lines:  $6\alpha$  ( $12.37\mu\text{m}$ ),  $7\alpha$  ( $19.06\mu\text{m}$ ) and  $8\alpha$  ( $27.80\mu\text{m}$ ). They arise from high-level transitions:  $n = 7 \rightarrow 6$ ,  $n = 8 \rightarrow 7$ , and  $n = 9 \rightarrow 8$ , respectively. However, as we will show below, these lines and in fact most H I transitions also contain a contribution of He I or He II lines, depending on the spectral type (or, more precisely, of the effective temperature).

The hottest two stars, with spectral types O4, also show a few individual lines of He II, most intense at  $13.13\mu\text{m}$  (11-10),  $17.26\mu\text{m}$  (12-11),  $22.17\mu\text{m}$  (13-12), and significantly weaker at  $15.47\mu\text{m}$  (15-13),  $16.77\mu\text{m}$  (18-15). Note that the line at  $17.26\mu\text{m}$  is also observed in HD 207198, despite its much later spectral type (O8.5). The use of models allowed to pinpoint this line, as it is weak and not much stronger than the noise level in surrounding zones.

<sup>1</sup> We note that our best models initially predicted a relatively intense H I line at  $13.19 \mu\text{m}$  ( $n = 18 \rightarrow 10$ ), which is absent in all observed spectra. After some investigation, we found that the  $f$  and  $A$  values for this transition in the CMFGEN atomic database is higher than it should be by a factor of 10, according to the NIST database (Kramida et al. 2015; John Hillier, private comm.).

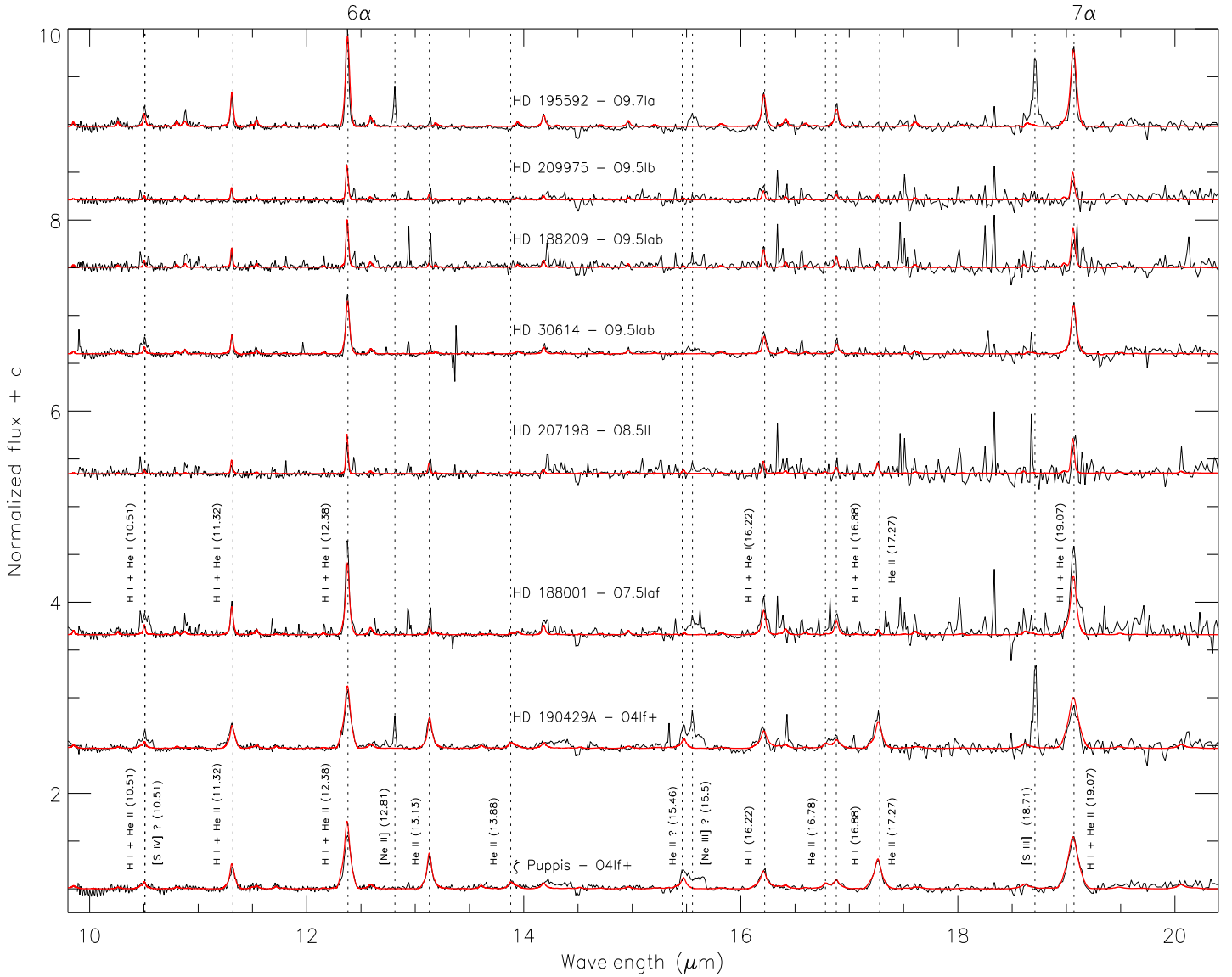


**Figure 1.** The mid-IR *Spitzer* spectra of the supergiants of our sample, between 9.8 and 20.4  $\mu\text{m}$  (black lines), with early-type to late-type supergiants from bottom to top. Synthetic CMFGEN spectra are also displayed (red lines). They are essential to characterize quantitatively the mid-IR spectrum, providing the line identifications shown, individual ion contributions and line formation regions (see text for more details).

We present a detailed list of line identifications and  $W_\lambda$  measurements in Table A2. In some cases, no reliable  $W_\lambda$  could be obtained (e.g., weak or blended feature). Therefore, the respective line identifications on the table should be then interpreted as an indication that a line is likely present, based on the overlying models. These results are summarized in graphical form in Fig. 3, where we present mean equivalent widths of the late plus mid ( $\geq O7$ ) and earlier supergiants classes. The  $W_\lambda$  values increase from late to the early supergiants. It is clear that early supergiants have the most intense lines. Moreover, regardless of the spectral class, the most intense features are always  $6\alpha$ ,  $7\alpha$ , and  $8\alpha$ .

We did not identify metallic lines (e.g., from CNO ions)

in a definitive way, in contrast to spectral features observed in the near-IR. For example, [Hanson et al. \(1996\)](#) report lines of C IV and N III in several O stars spectra around  $2\mu\text{m}$ . The lines that are not accounted for by our model spectra are unlikely to be formed in the atmosphere of the stars. This is for instance the case of the features between  $\sim 16 - 19\mu\text{m}$ , most clearly visible in the mid-to-late supergiants, and for which we could not find any identification in the literature (see Fig. 1). We do not exclude the possibility that some of them might be artifacts that remained despite the data reduction process. The features at  $\sim 15.5\mu\text{m}$  and close to  $26\mu\text{m}$  (box-like shape) are also clear discrepancies. They are both conspicuous in  $\zeta$  Puppis and HD 190429A (see Figs. 1



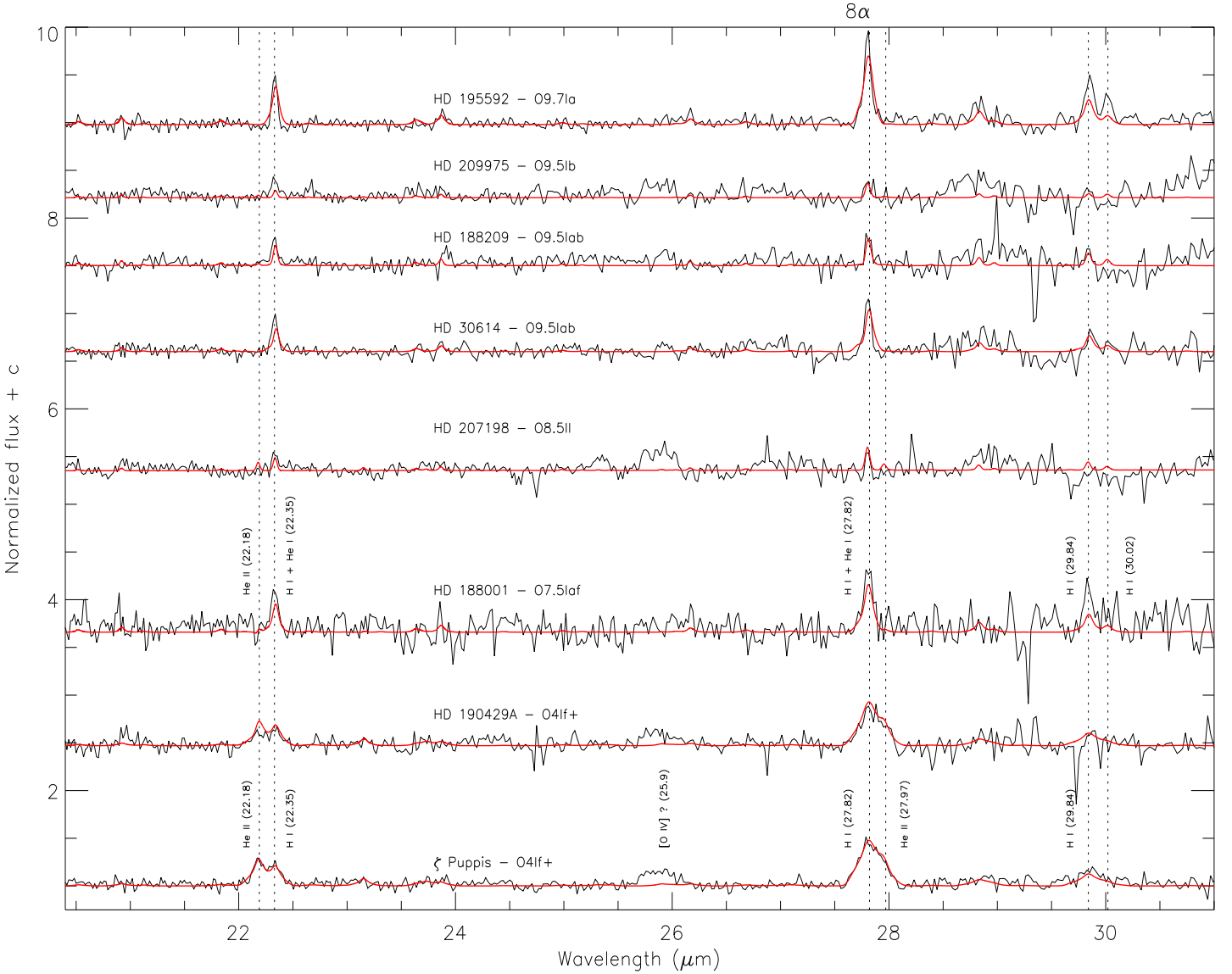


**Figure 2.** Same as Fig. 1 but for the spectral region between 20.4 and 31.0  $\mu\text{m}$ .

and 2). They were also reported in the *Spitzer* observations of EZ Canis Majoris, a WN star, by Morris et al. (2004) who identified them to [Ne III] 15.5  $\mu\text{m}$  and [O IV] 25.9  $\mu\text{m}$  transitions.

The [S IV] 10.5  $\mu\text{m}$ , [Ne II] 12.8  $\mu\text{m}$ , and [S III] 18.7  $\mu\text{m}$  lines, are also possibly present in some spectra, e.g. in HD 190429A and HD 195592. These two stars are known binaries. The respective companions of each were certainly in the field of view of the SH and LH modules during observations, but it remains speculative to assume that the companions are responsible for the observed features. We note that HD 195592 has a very high reddening ( $E(B-V) = 1.17$ , see McSwain et al. 2007), indicating that lots of interstellar/circumstellar material is on the line-of-sight. Hence we are tempted to assume that the emission features are produced around HD 195592. Interpreting their presence in

HD 190429A is more difficult as  $E(B-V) = 0.46$  (Bouret et al. 2012) and is nothing exceptional even for early-type supergiants. In any case, such fine-structure transitions must be formed far from the bulk of the stellar wind, where densities are very low ( $\log n_e/\text{cm}^3 \sim 5$ ).

Despite our efforts, several non-atmospheric features remained unidentified. We note that the signal-to-noise starts to deteriorate beyond 28  $\mu\text{m}$  and it becomes hard to confirm the presence of lines at longer wavelengths, regardless the origin.

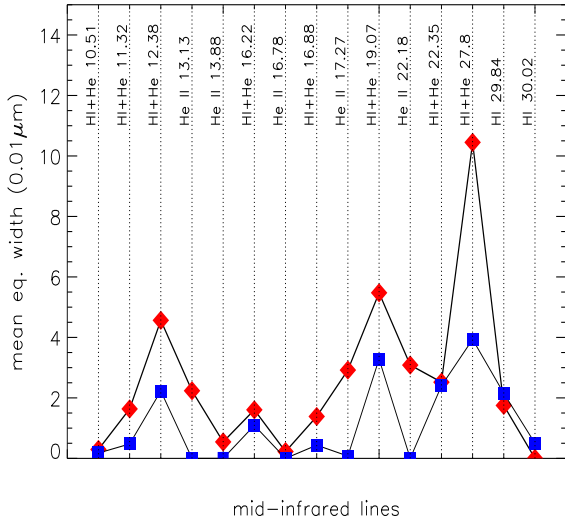


**Figure 3.** Mean equivalent widths of mid plus late-type O supergiants ( $\geq O7$ ; squares; thin solid line) and early-type O supergiants (diamonds; thick solid line). Note that the highest values correspond to the wavelengths of the  $6\alpha$ ,  $7\alpha$ , and  $8\alpha$  transitions. The He II transitions at  $13.13\mu\text{m}$ ,  $17.27\mu\text{m}$ , and  $22.18\mu\text{m}$ , clearly separate early-type objects from later-type stars.

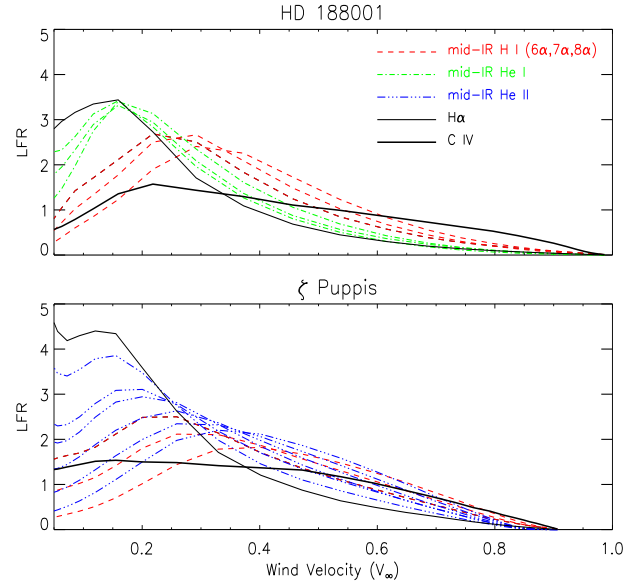


**Figure 5.** Line formation regions in O supergiants. The H I transitions are the mid-IR ( $6\alpha$ ,  $7\alpha$ , and  $8\alpha$ ) and H $\alpha$ . The He I and He II transitions chosen are at  $\sim 12.36$ ,  $19.06$ , and  $27.9\mu\text{m}$ , i.e., at wavelengths corresponding to  $6\alpha$ ,  $7\alpha$ , and  $8\alpha$ . He II transitions at  $13.13$ ,  $17.26$ , and  $22.17\mu\text{m}$  are also shown.

### 3.1.1 Line contributions and formation regions

Following our methodology to identify the transitions in the spectra<sup>2</sup>, we found that the profiles  $6\alpha$ ,  $7\alpha$ , and  $8\alpha$  (the most intense ones) are contaminated by a He I-II contribution, as illustrated in Fig. 4. For simplicity, we selected regions comprising the  $6\alpha$  and  $8\alpha$  lines and show only synthetic models for HD 188001 (O7.5Iaf) and  $\zeta$  Puppis (O4If+) as examples. In early O supergiants, the full line profiles are formed by a contribution of H I and He II. The He I contribution is negligible. The He II contribution to  $8\alpha$  is particularly important, and is responsible for the asymmetry of the line profile. In mid and late supergiants, we see the opposite: the profiles mostly result from the H I transition, with a small contribution of He I, and He II is absent. *These characteristics of the mid-IR line spectra were more clearly evidenced thanks to the stellar atmosphere models.*

Overall, from the observations and model spectra, we conclude that: (i) the early supergiants have the most intense transitions in the mid-IR; (ii) mid and late supergiants present the main features composed by H I and He I lines; (iii) early supergiants present the main features composed by H I and He II lines, He I lines being absent; (iv) the most intense transitions are from H I  $6\alpha$ ,  $7\alpha$ , and  $8\alpha$ .

Now, we present the line formation regions (LFRs) for specific lines. Regarding H I lines, we chose  $6\alpha$ ,  $7\alpha$ , and  $8\alpha$ . The He I and He II transitions chosen are at  $\sim 12.36$ ,  $19.05$ , and  $27.9\mu\text{m}$ . Besides mid-IR transitions, for comparison purposes, we compute LFRs for the C IV  $\lambda 1551$  and H $\alpha$  profiles. We refer the reader to Hillier (1987) for an expression for the quantity that defines the LFR.

<sup>2</sup> We have computed synthetic spectra produced by individual ions and checked the corresponding wavelengths.

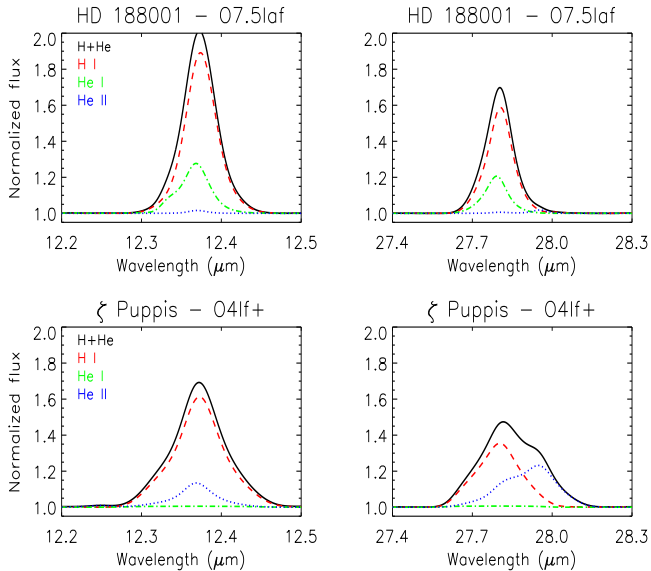


**Figure 4.** Individual ion contributions to the most intense mid-IR profiles in O supergiants. Top panels correspond to HD 188001 (O7.5Iaf). Bottom panels correspond to  $\zeta$  Puppis (O4If+). For clarity, only the synthetic lines  $6\alpha$  and  $8\alpha$  are shown (full spectrum: black full line; H I: red dashed line; He I: green dashed-dotted line; He II: blue dotted line).

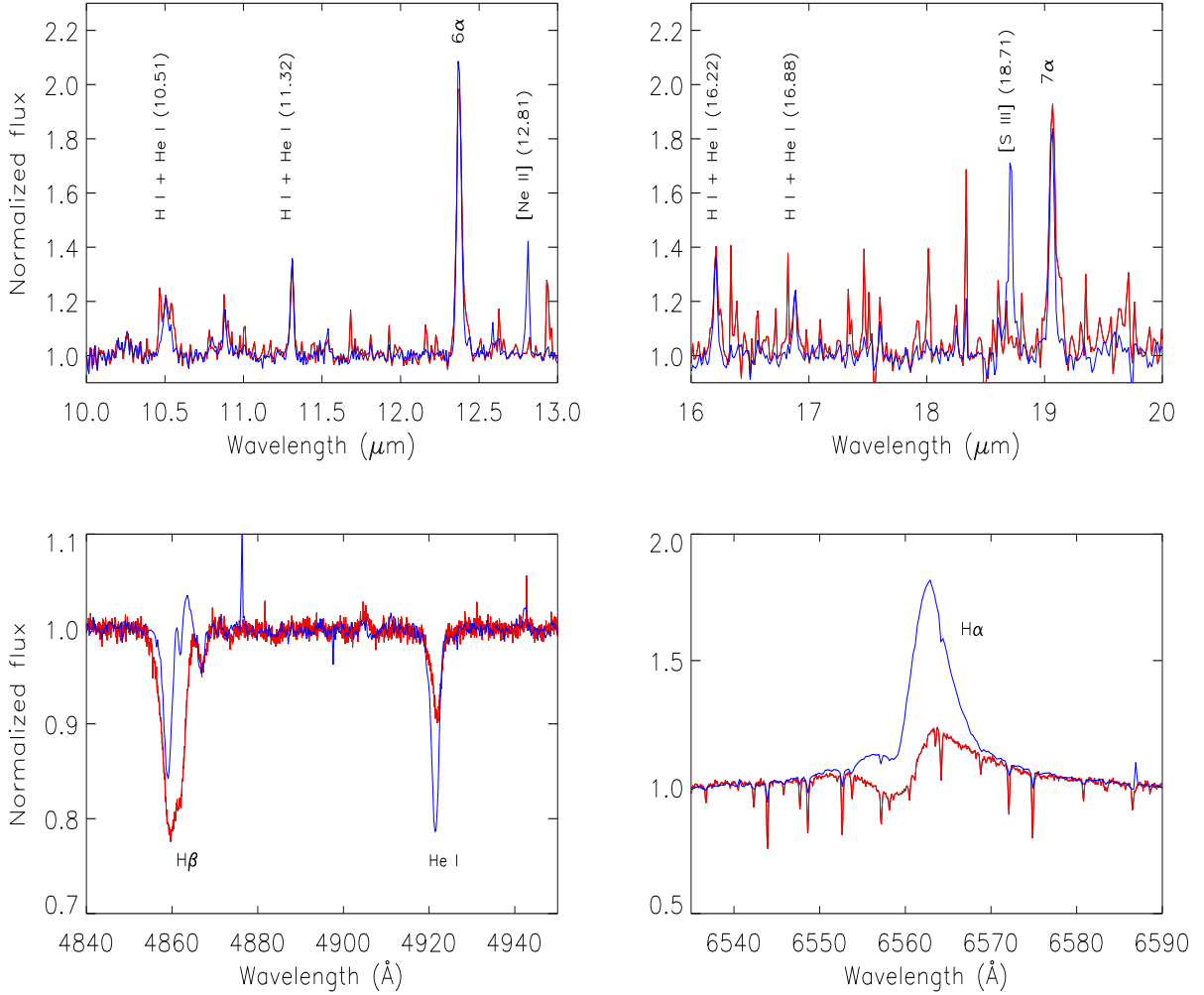


**Figure 6.** The similar mid-IR (top) and drastically different optical spectra (bottom) of HD 195592 (O9.7Ia, blue lines) and HD 188001 (O7.5Iaf, red lines). Note that the mid-IR mismatches - in particular around 16-20 $\mu\text{m}$  - are likely due to non-atmospheric features, as discussed in Section 3.

For simplicity, we present LFRs in Fig. 5 for two stars, again HD 188001 (O7.5Iaf) and  $\zeta$  Puppis (O4If+). It can be seen that  $6\alpha$ ,  $7\alpha$ , and  $8\alpha$  follows the C IV ultraviolet line trend, being formed throughout the wind. The bulk of the He I lines (in mid and late-type supergiants) is formed in the inner wind, similar to H $\alpha$ . The He II LFRs (in early-type supergiants) follow more or less the ones of the mid-IR H I lines.

In conclusion, *our results demonstrate that the observed mid-IR features in O supergiants are definitely formed in the stellar wind. Therefore, they are potential diagnostics for the determination of wind properties.* A detailed analysis of mid-IR line responses to the different physical parameters is beyond the scope of the present paper and will be presented elsewhere. Here, we just emphasize that the same value for the mass-loss rate (and clumping parameters) allows us to match simultaneously the UV P-Cygni profiles, H $\alpha$ , and the mid-IR lines, as demonstrated for  $\zeta$  Puppis (appendix, Fig. A2).

### 3.1.2 The case of the two supergiants HD 195592 and HD 188001

From a pure morphological, mid-IR point of view, HD 195592 is at odds with its spectral classification, namely, O9.7 Ia. While its fellow late-type O9 (and sub-division) supergiants exhibit weaker lines than the earlier type ones, the lines in HD 195592 are remarkably similar in shape and intensity to those of HD 188001, an O7.5 Iaf. This is best illustrated in Fig. 6, where we overplot a selection of lines from the mid-IR spectra of the two stars (but see also Figs. 1 and 2 for a pan view). We also show portions of the optical spectra, demonstrating that these stars are very different one of the other, in agreement to their spectral classification.

A low-resolution UV (IUE) spectrum for HD 195592 is available and despite the modest signal-to-noise ratio, exhibits spectral morphology consistent with the star's O9.7 Ia spectral type. So we are facing here an interesting conundrum, and taken at face value, these two stars demonstrate that the mid-IR range should be used with caution to assign a spectral type to a massive supergiant star, at least in the



range from O7.5 to O9.7 (where most supergiants are expected to belong). This is specially important in the context of observations of heavily obscured regions.

Despite this seemingly paradoxical behavior, models can be found that simultaneously fit the UV, optical, and mid-IR spectra. The parameters from these models can be found in Table A1. The model parameters are fully compatible with the results found in the literature for stars of these spectral types, hence clearly suggesting a spectral degeneracy in the mid-IR (different stellar parameters but very similar spectra). This issue deserves a deeper theoretical investigation that is beyond the scope of this paper.

In contrast to the arguments presented above, one can argue that (drastic) variability (O9 to O7) is a possible explanation for the atypical spectrum of HD 195592. Variability of HD 195592 from an "normal" mid-IR O9 spectrum (i.e., like the others O9 in the sample) to an O7 spectrum (matching HD 188001) and back (if periodic) would be drastic, but not impossible. Binarity effects, wind instabilities, and wind collisions are all possibilities to produce spectral changes. If this is the case, our observations would then correspond to HD 195592 at the spectral state of an O7 (HD 188001). We note however that the SH and LH spectra of HD 195592 (and of HD 188001) were acquired at different dates (see Table 1). That is, in Figs. 1 and 2 we actually have four spectra. If variability is very important, similar spectra would be unlikely.

### 3.2 O dwarfs

The mid-IR spectra of O dwarfs - late, mid and early types - are featureless, that is, with an absence of conspicuous lines formed in the photosphere or in the stellar wind. For completeness, they are presented in Fig. A3 along with our model stellar atmosphere spectra, adopted from an UV/optical analysis.

The spectrum of HD 38666 has a very low signal-to-noise ratio at wavelengths longer than  $15\mu\text{m}$ , hindering the analysis. The 10 Lac spectrum is of better quality, but it does not show either stellar or wind transitions. In HD 209481, the atmospheric transitions  $6\alpha$ ,  $7\alpha$  and  $8\alpha$  are barely visible, if present at all. We recall that they are the strongest features in the spectra of O supergiants. Forbidden lines seem to be present in a few stars (e.g., [O IV]) and various narrow unidentified transitions are conspicuous.

Although more luminous, hotter, and with higher mass-loss rates than O9V stars, the O4-7V stars of our sample also present a featureless spectra. Again, various (non-atmospheric) features at  $\sim 17\text{-}19\mu\text{m}$  and  $\sim 23\text{-}27\mu\text{m}$  (see e.g., HD 199579), as well as [O IV]  $25.9\mu\text{m}$  (see e.g., HD 206267) are present.

The results concerning the early dwarfs (O4-5V) are somewhat counterintuitive. Since their ultraviolet spectra contain intense wind emission lines - e.g., C IV  $\lambda\lambda 1548, 1551$  can be even found saturated, as in supergiants - one would expect at least weak emissions in the mid-IR. In fact, their effective temperature and luminosity values are even compatible with the ones found in early supergiants (see Table A1). We must remind however that their surface gravities are higher by up to 1 dex relative to supergiants and most importantly, the mass-loss rates of the O supergiants can be higher by 1-2 dex. Therefore, it seems that a combination of

low gravity and intense mass-loss is needed for a detectable mid-IR line emission spectrum. Nevertheless, a firmer conclusion awaits a more detail theoretical study.

Overall, *we conclude that there is no atmospheric information regarding O dwarfs in the mid-IR beyond the continuum flux level.* The observed features are likely formed far from their atmospheres, being circumstellar or even from the ISM (e.g., diffuse emission). Some are certainly spurious, given the limited signal-to-noise achieved for some stars (see e.g., HD 38666 and HD 199579 at  $\sim 29\mu\text{m}$ ). Our models give confidence to this conclusion since they reveal pure mid-IR continua. This finding should be taken into account in future investigations. For example, it does not appear useful to acquire mid-IR spectra of main-sequence stars in regions with extremely high visual extinction at high cost with the MIRI instrument aboard the JWST.

## 4 CONCLUSIONS

We have presented an analysis of mid-IR data of O-type stars, based on observations with the NASA *Spitzer Space Telescope* (IRS instrument;  $R \sim 600$ ). We provided a detailed description of the spectra supported by model spectra from NLTE expanding model atmospheres calculated with the CMFGEN code.

We found that O supergiants present a rich emission line mid-IR spectrum, while O dwarfs are essentially featureless in terms of atmospheric information. The most intense transitions found in O supergiants are the H I recombination lines:  $6\alpha$  ( $n = 7 \rightarrow 6$ ;  $12.37\mu\text{m}$ ),  $7\alpha$  ( $n = 8 \rightarrow 7$ ;  $19.06\mu\text{m}$ ), and  $8\alpha$  ( $n = 9 \rightarrow 8$ ;  $27.80\mu\text{m}$ ). However, according to our models, these lines have a non-negligible contribution of He I lines in mid and late O supergiants, and of He II lines in early O supergiants. In early O-type supergiants, the He II line contribution is responsible for the asymmetry of the  $8\alpha$  line profile.

We provided line identifications and measurements for all detected H I, He I, and He II features (Table A2). The presence of isolated, relatively strong He II lines at  $13.13\mu\text{m}$ ,  $17.27\mu\text{m}$ , and  $22.18\mu\text{m}$ , is a basic characteristic of early-type supergiant spectra. We do not identify lines from heavy element ions (e.g., CNO) formed in the stellar photosphere or wind, in contrast to the near-IR spectrum. There are however several features that are probably of circumstellar origin, e.g., [Ne III]  $15.5\mu\text{m}$  and [O IV]  $25.9\mu\text{m}$ . Despite our efforts, a few detected emission features remain unidentified.

Two supergiants - HD 188001 and HD 195592 - raised an interesting problem. Their mid-IR spectra are very similar while their optical characteristics drastically differ. From a pure observational point of view, such fact means that the use of mid-IR data alone to classify O stars may be prone to errors if unsupported by observations in UV, optical or near-IR. This must be taken into account in observations of heavily-obscured regions (e.g., the Galactic Center, obscured H II regions). Additionally, the lack of photospheric or wind features in the mid-IR spectrum of all O dwarfs put a stringent limitation about the usefulness of such observations. In regions inaccessible to UV or optical observations because of heavy extinction, the near-IR should be preferred to observe and analyze main-sequence massive stars.

## ACKNOWLEDGEMENTS

The authors would like to thank D. J. Hillier for his continuous support regarding CMFGEN. WM would like to thank J.-C. Bouret for the hospitality at the Laboratoire d'Astrophysique de Marseille, where part of the work was carried out. Support for this work was provided by NASA through an award issued by JPL/Caltech. This research also made use of the SIMBAD database and VizieR service, operated at CDS, Strasbourg, France.

## REFERENCES

- Ardila D. R., et al., 2010, *ApJS*, **191**, 301  
 Bouret J.-C., Lanz T., Hillier D. J., 2005, *A&A*, **438**, 301  
 Bouret J.-C., Hillier D. J., Lanz T., Fullerton A. W., 2012, *A&A*, **544**, A67  
 Conti P. S., Hanson M. M., Morris P. W., Willis A. J., Fossey S. J., 1995, *ApJ*, **445**, L35  
 Crowther P. A., Hillier D. J., Evans C. J., Fullerton A. W., De Marco O., Willis A. J., 2002, *ApJ*, **579**, 774  
 Hanson M. M., Conti P. S., Rieke M. J., 1996, *ApJS*, **107**, 281  
 Hillier D. J., 1987, *ApJS*, **63**, 965  
 Hillier D. J., Miller D. L., 1998, *ApJ*, **496**, 407  
 Hodge T. M., Kraemer K. E., Price S. D., Walker H. J., 2004, *ApJS*, **151**, 299  
 Houck J. R., et al., 2004, *ApJS*, **154**, 18  
 Howarth I. D., Prinja R. K., 1989, *ApJS*, **69**, 527  
 Kramida A., Ralchenko Y., Reader J., and NIST ASD Team 2015, NIST Atomic Spectra Database (ver. 5.3), [Online]. Available: <http://physics.nist.gov/asd> [2017, January 16]. National Institute of Standards and Technology, Gaithersburg, MD.  
 Lenorzer A., Mokiem M. R., de Koter A., Puls J., 2004, *A&A*, **422**, 275  
 Martins F., Marcolino W., Hillier D. J., Donati J.-F., Bouret J.-C., 2015a, *A&A*, **574**, A142  
 Martins F., et al., 2015b, *A&A*, **575**, A34  
 McSwain M. V., Boyajian T. S., Grundstrom E. D., Gies D. R., 2007, *ApJ*, **655**, 473  
 Morris P. W., Eenens P. R. J., Hanson M. M., Conti P. S., Blum R. D., 1996, *ApJ*, **470**, 597  
 Morris P. W., Crowther P. A., Houck J. R., 2004, *ApJS*, **154**, 413  
 Morton D. C., 1967, *ApJ*, **147**, 1017  
 Najarro F., Hanson M. M., Puls J., 2011, *A&A*, **535**, A32  
 Prinja R. K., Howarth I. D., 1986, *ApJS*, **61**, 357  
 Puls J., Markova N., Scuderi S., Stanghellini C., Taranova O. G., Burnley A. W., Howarth I. D., 2006, *A&A*, **454**, 625  
 Repolust T., Puls J., Hanson M. M., Kudritzki R.-P., Mokiem M. R., 2005, *A&A*, **440**, 261  
 Sota A., Maíz Apellániz J., Morrell N. I., Barbá R. H., Walborn N. R., Gamen R. C., Arias J. I., Alfaro E. J., 2014, *ApJS*, **211**, 10  
 Teplitz H., Brinkworth C., 2011, SPICE User's Guide (ver. 2.3.1), [Online]. Available: <http://irsa.ipac.caltech.edu/> [2017, March 17] NASA/IPAC Infrared Science Archive.  
 Walborn N. R., Panek R. J., 1984, *ApJ*, **280**, L27  
 Wright A. E., Barlow M. J., 1975, *MNRAS*, **170**, 41

**APPENDIX A: ADDITIONAL DATA**

This paper has been typeset from a  $\text{\TeX}/\text{\LaTeX}$  file prepared by the author.

**Table A1.** Stellar and wind parameters of the sample. Values for additional physical (and chemical) parameters can be found in the quoted references: (1) this work; (2) Martins et al. (2015a); (3) Martins et al. (2015b); (4) Bouret et al. (2012). The uncertainty for  $T_{eff}$  is about  $\pm 2000K$ ,  $\log g$  is  $\pm 0.1$ ,  $v_\infty$  is about  $\sim 200 \text{ km s}^{-1}$ , and  $\dot{M}$  is  $\sim 0.4$  dex.

Star	Spec. type	$T_{eff}$ (kK)	$\log g$ (cgs)	$L_\star$ ( $L_\odot$ )	$\log \dot{M}$ ( $M_\odot \text{ yr}^{-1}$ )	$f_{cl}$	$V_\infty$ ( $\text{km s}^{-1}$ )	$\beta$	Ref.
HD 66811	O4If+	41.0	3.6	$5.92 \pm 0.10$	-5.70	0.05	2300	0.9	1,4
HD 190429A	O4If+	39.0	3.6	$5.97 \pm 0.10$	-5.64	0.04	2300	1.0	1,4
HD 188001	O7.5Iaf	33.0	3.4	$5.69 \pm 0.20$	-5.88	0.05	1800	1.5	1
HD 207198	O8.5II	32.5	3.5	$5.05 \pm 0.26$	-7.00	1.0	2000	3.0	1,2
HD 30614	O9.5Iab	28.9	3.0	$5.81 \pm 0.25$	-5.62	0.1	1600	1.2	1
HD 188209	O9.5Iab	29.8	3.2	$5.65 \pm 0.26$	-6.40	0.05	2000	2.2	1,2
HD 209975	O9.5Ib	30.5	3.3	$5.35 \pm 0.30$	-6.50	1.0	2000	2.9	1,2
HD 195592	O9.7Ia	28.0	2.9	$5.47 \pm 0.25$	-5.79	0.05	1400	1.4	1
HD 46223	O4V((f))	43	4.0	$5.60 \pm 0.25$	-7.20	0.1	2800	1.0	3
HD 46150	O5V((f))	42	4.0	$5.60 \pm 0.25$	-7.30	0.1	2800	1.0	3
HD 199579	O6V((f))	41.5	4.15	$5.33 \pm 0.25$	-7.84	0.1	2750	0.8	1,3
HD 206267	O6.5V((f))	39.0	4.0	$5.20 \pm 0.25$	-7.49	0.5	2750	0.8	1
HD 47839	O7V((f))	37.0	4.0	$5.15 \pm 0.25$	-8.00	1.0	2000	1.0	1
HD 209481	O9V	31.5	3.9	$4.72 \pm 0.25$	-8.70	1.0	1600	0.8	1
HD 214680	O9V	35.0	4.0	$4.34 \pm 0.25$	-9.52	1.0	1200	0.8	1,3
HD 38666	O9.5V	33.0	4.0	$4.68 \pm 0.25$	-9.82	1.0	1200	1.0	1,3

**Table A2.** Line identifications and equivalent width measurements of the mid-IR features of the O supergiants.

Star	Observed $\lambda(\mu m)$	Identification	Rest Wavelength $\lambda(\mu m)$	$W_\lambda (\mu m \cdot 10^{-2})$
HD 66811 ( $\zeta$ Pup)	10.51	H I + He II	10.50 + 10.47	$0.59 \pm 0.01$
	11.32	H I + He II	11.31 + 11.33	$1.28 \pm 0.04$
	12.38	H I + He II	12.37 + 12.38	$4.50 \pm 0.07$
	13.13	He II	13.13	$2.33 \pm 0.04$
	13.88	He II	13.87	$0.52 \pm 0.04$
	15.46	He II	15.47	-
	16.22	H I	16.21	$1.94 \pm 0.03$
	16.78	He II	16.77	$0.45 \pm 0.03$
	16.88	H I	16.88	$1.26 \pm 0.09$
	17.27	He II	17.26	$2.82 \pm 0.07$
	19.07	H I + He II	19.06 + 19.05	$6.30 \pm 0.04$
	22.18	He II	22.17	$3.44 \pm 0.10$
	22.35	H I	22.33	$3.15 \pm 0.12$
	27.82 + 27.97	H I + He II	27.80 + 27.95	$12.28 \pm 0.11$
	29.84	H I	29.84	$3.50 \pm 0.50$
	HD 190429A	10.51	H I + He II	10.50 + 10.47
11.32		H I + He II	11.31 + 11.33	$1.99 \pm 0.12$
12.38		H I + He II	12.37 + 12.38	$4.63 \pm 0.07$
13.13		He II	13.13	$2.14 \pm 0.03$
13.88		He II	13.87	$0.57 \pm 0.02$
15.46		He II	15.47	-
16.22		H I	16.21	$1.27 \pm 0.03$
16.88		He II + H I	16.77 + 16.88	$1.51 \pm 0.03$
17.28		He II	17.26	$3.02 \pm 0.03$
19.08		H I + He II	19.06 + 19.05	$4.65 \pm 0.16$
22.19		He II	22.17	$2.73 \pm 0.04$
22.33		H I	22.33	$1.89 \pm 0.23$
27.82		H I + He II	27.80 + 27.95	$8.62 \pm 0.13$
29.84		H I	29.84	-
HD 188001		10.51	H I + He I	10.50
	11.32	H I + He I	11.31 + 11.30	$1.05 \pm 0.02$
	12.38	H I + He I	12.37 + 12.39	$4.55 \pm 0.01$
	16.22	H I + He I	16.21 + 16.20	$2.38 \pm 0.04$
	16.88	H I + He I	16.88	$1.10 \pm 0.20$
	19.07	H I + He I	19.06 + 19.05	$7.82 \pm 0.03$
	22.35	H I + He I	22.33 + 22.32	$3.88 \pm 0.07$
	27.81	H I + He I	27.80 + 27.79	$7.40 \pm 0.20$
	29.84	H I	29.84	$5.00 \pm 0.30$
	HD 207198	11.32	H I	11.31
12.38		H I + He I	12.37 + 12.39	$0.81 \pm 0.02$
17.27		He II	17.26	$0.46 \pm 0.01$
19.07		H I + He I	19.06 + 19.05	$1.49 \pm 0.10$
22.19		He II	22.17	-
22.35		H I + He I	22.33 + 22.32	$1.29 \pm 0.04$
27.82		H I + He I	27.80 + 27.79	$0.65 \pm 0.18$

Table A2 – continued

Star	Observed $\lambda(\mu\text{m})$	Identification	Rest Wavelength $\lambda(\mu\text{m})$	$W_\lambda (\mu\text{m} \cdot 10^{-2})$
HD 30614 ( $\alpha$ Cam)	10.51	H I + He I	10.50	-
	11.32	H I + He I	11.31 + 11.30	$0.45 \pm 0.01$
	12.38	H I + He I	12.37 + 12.39	$2.56 \pm 0.05$
	16.22	H I + He I	16.21 + 16.20	$1.32 \pm 0.03$
	16.88	H I + He I	16.88 + 16.87	$0.55 \pm 0.01$
	19.07	H I + He I	19.06 + 19.05	$3.07 \pm 0.10$
	22.35	H I + He I	22.33 + 22.32	$2.56 \pm 0.04$
	27.82	H I + He I	27.80 + 27.79	$4.17 \pm 0.04$
	29.84	H I	29.84	$1.70 \pm 0.20$
	30.02	H I	30.02	-
	HD 188209	10.51	H I + He I	10.50
11.32		H I + He I	11.31 + 11.30	$0.21 \pm 0.03$
12.38		H I + He I	12.37 + 12.39	$1.36 \pm 0.05$
16.22		H I + He I	16.21 + 16.20	$0.71 \pm 0.04$
19.07		H I + He I	19.06 + 19.05	$1.45 \pm 0.22$
22.35		H I + He I	22.33 + 22.32	$2.21 \pm 0.13$
27.82		H I + He I	27.80 + 27.79	$1.96 \pm 0.03$
29.84		H I	29.84	$1.10 \pm 0.10$
HD 209975	11.32	H I + He I	11.31 + 11.30	$0.17 \pm 0.02$
	12.38	H I + He I	12.37 + 12.39	$1.02 \pm 0.04$
	16.22	H I + He I	16.21 + 16.20	$0.80 \pm 0.02$
	19.07	H I + He I	19.06 + 19.05	$1.05 \pm 0.04$
	22.35	H I + He I	22.33 + 22.32	$1.66 \pm 0.22$
	27.82	H I + He I	27.80 + 27.79	$1.01 \pm 0.29$
HD 195592	10.51	H I + He I	10.50 + 10.50	$1.06 \pm 0.03$
	11.32	H I + He I	11.31 + 11.30	$0.84 \pm 0.01$
	12.38	H I + He I	12.37 + 12.39	$4.06 \pm 0.05$
	16.22	H I + He I	16.21 + 16.20	$1.33 \pm 0.05$
	16.88	H I + He I	16.88 + 16.87	$0.97 \pm 0.01$
	19.07	H I + He I	19.06 + 19.05	$4.83 \pm 0.23$
	22.35	H I + He I	22.33 + 22.32	$2.80 \pm 0.05$
	27.82	H I + He I	27.80 + 27.79	$8.42 \pm 0.41$
	29.84	H I	29.84	$5.10 \pm 0.30$
	30.02	H I	30.02	$3.00 \pm 0.30$



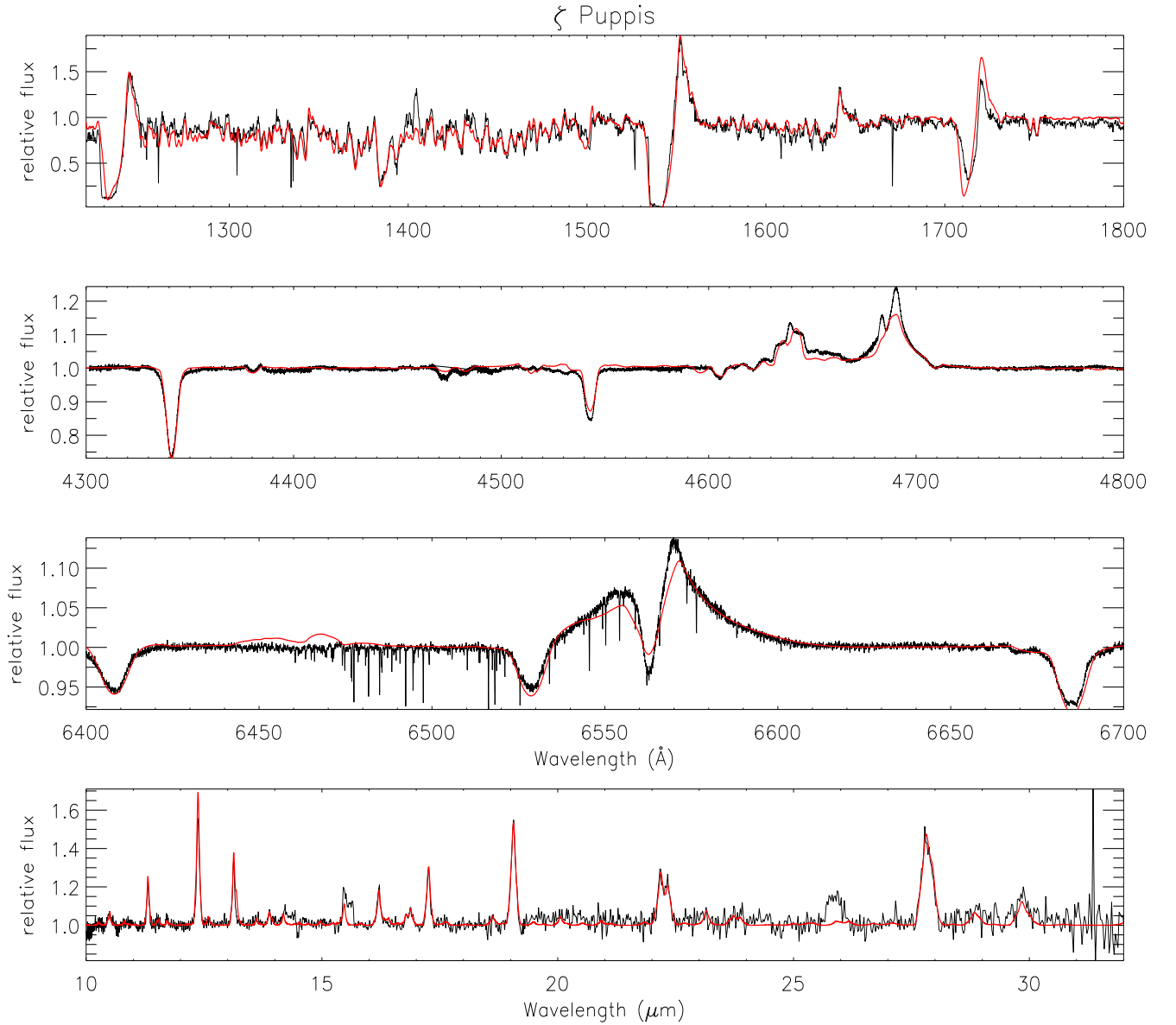


**Figure A1.** Model fits (red; thick line) to the UV (IUE), optical (FEROS) and mid-IR (Spitzer) data of  $\zeta$  Puppis.

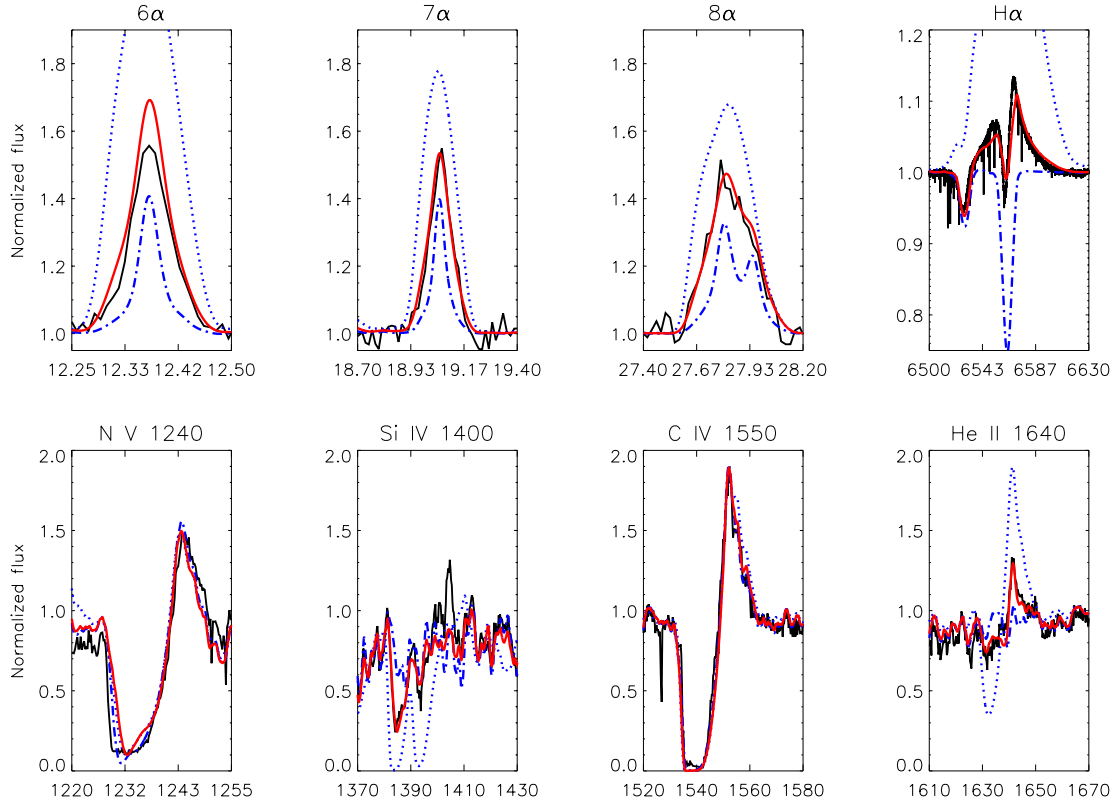


**Figure A2.** Sensitivity of mid-IR lines to mass-loss rate changes (wavelength given in  $\mu\text{m}$ ). The chosen star is  $\zeta$  Puppis. Selected UV lines and H $\alpha$  are also shown (wavelengths in  $\text{\AA}$ ). The rates displayed are:  $7.0 \times 10^{-7} M_{\odot} \text{ yr}^{-1}$  (blue dashed-dotted line),  $1.9 \times 10^{-6} M_{\odot} \text{ yr}^{-1}$  (final model; red solid line), and  $6.0 \times 10^{-6} M_{\odot} \text{ yr}^{-1}$  (blue dotted line). A unique model spectrum with the same mass-loss rate matches the mid-IR, optical and UV observations (black).

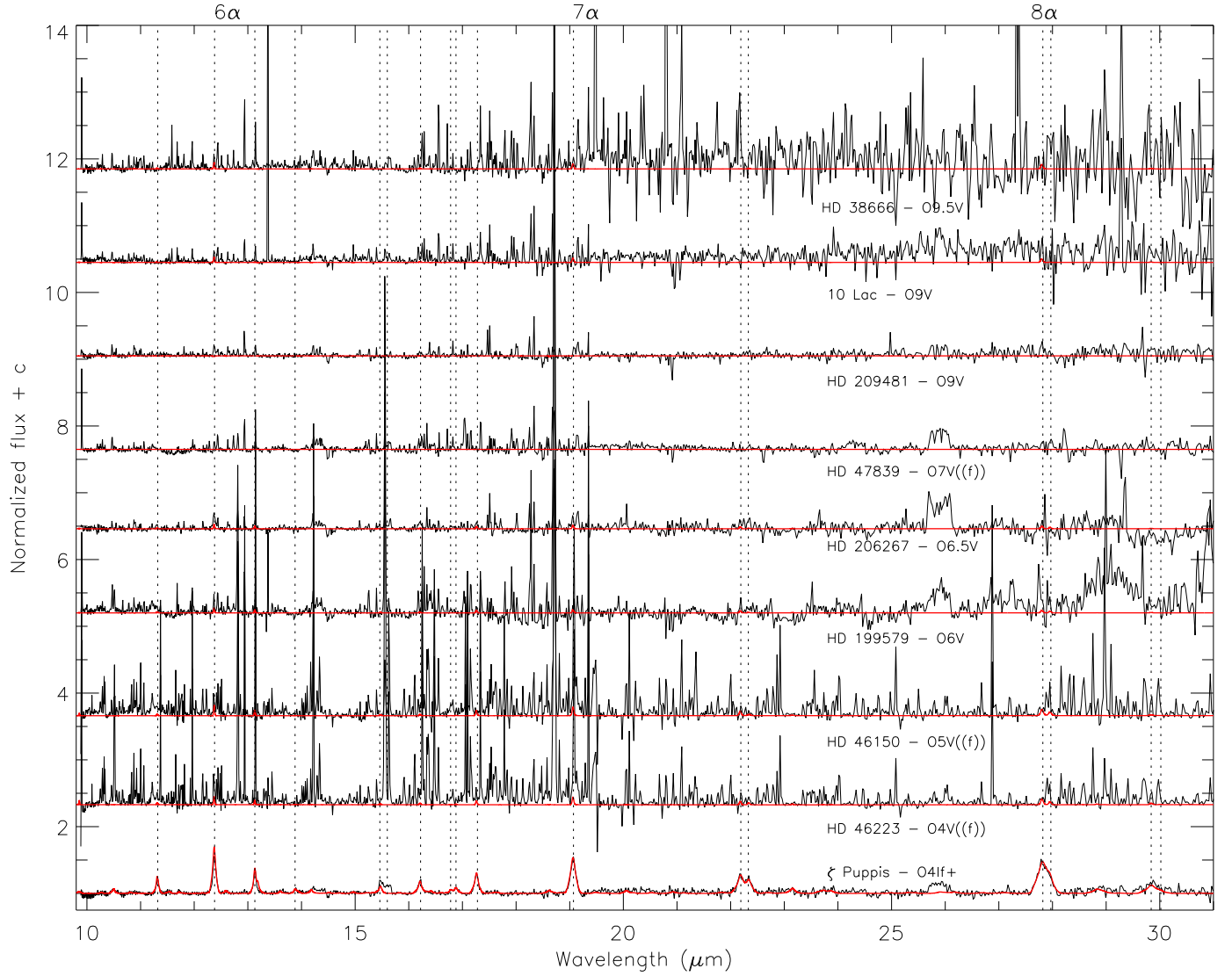


**Figure A3.** The mid-IR *Spitzer* spectra of the dwarfs of our sample (black lines). For comparison, the bottom panel show the observed and synthetic spectra of  $\zeta$  Puppis. From bottom to top we have early to late spectral types. Synthetic CMFGEN spectra are displayed in red. They support the conclusion that the mid-IR spectrum of O dwarfs does not contain conspicuous atmospheric features.